Contribution from the Chemistry Department,
State University of New York at Buffalo, Buffalo, New York 14214

Low-Temperature Electron Density Study of Thiotrithiazyl Nitrate, a Structure with a Short Contact between an Oxygen Atom and the Disulfide Group

GRANT MOSS,* T. N. GURU ROW, and PHILIP COPPENS*

Received December 19, 1979

Thiotrithiazyl nitrate crystals ($P2_1/n$, a = 5.7526 (5) Å, b = 10.3853 (9) Å, c = 11.868 (2) Å, β = 100.29 (1)° at 90 K) contain short interionic contacts between the disulfide group and a nitrate group oxygen atom. The experimental electron distribution, determined by low-temperature X-ray diffraction, shows the density in the close-contact region to be diffuse. This and the contraction of the short contacts on cooling are interpreted as evidence of a weak interaction, which however is accompanied by a charge transfer from the nitrate group to the thiotrithiazyl ion, leading to approximate neutrality of both groups as measured by electron-counting techniques. The electron density maps are in reasonable agreement with a theoretical map calculated by Johansen, except in the lone-pair regions of the chemically equivalent N(2) and N(3) atoms where the experiment shows little density, while for the N(1) atom opposite the disulfide group both theory and experiment indicate a clear lone-pair peak. In addition to the conventional refinement high-order and aspherical-atom (multipole) refinements were made. Model maps based on the least-squares multipole expansions give evidence for the incompleteness of the set of density functions in the region of the sulfur atoms.

Introduction

The cyclic thiotrithiazyl cation ($S_4N_3^+$) is one of a number of species summarized by Hordvik[1] in which the disulfide group forms a short intermolecular contact with an electron donor. In the case of $S_4N_3^+$ the external atom may be a chlorine, bromine, iodine, or oxygen and lies in general in or close to the plane of the π-bonded cation. The interaction has been described as a weak two-electron three-center bond with a partial transfer of charge from a filled orbital on the electron donor to an empty orbital on the sulfur atom.[1] An extensive survey by Rosenfield, Parthasarathy, and Dunitz,[2] more recently extended by Guru Row and Parthasarathy,[3] shows that electron donors approach sulfur atoms in the plane of the atom and its adjacent bonds, in agreement with the above interpretation.

The present low-temperature study was undertaken to provide experimental evidence for the nature of this interaction, the amount of charge transfer involved, and the electronic structure of $S_4N_3^+$, from the experimental charge density distribution. A preliminary room-temperature study has been reported previously.[4]

Experimental Section

Crystals of $S_4N_3NO_3$ were prepared by slow cooling of a solution of thiotrithiazyl chloride in hot fuming nitric acid. The yellow crystals were mounted in Lindemann glass capillaries. Intensity data were collected at liquid-nitrogen temperature (90 K) on a Picker FACS-I four-circle diffractometer in the θ-2θ step scan mode using Nb-filtered Mo Kα radiation. Due to specimen deterioration during the course of the experiment three separate crystals were measured. In each case the (hkl) and $(\bar{h}kl)$ quadrants were collected. In the case of crystal 3 a further quadrant, the $(hk\bar{l})$ quadrant, was also measured. Nine standard reflections, collected after every 100 reflections, showed long-term fluctuations in intensity. Crystallographic information is given in Table I.

Data Reduction. Each of the separate data sets were reduced in the following manner. Reflection profiles were analyzed by using the method of Blessing, Coppens, and Becker[5] with the minimal $\sigma(I)/I$ criterion of Lehmann and Larsen.[6] Corrections for absorption were made by numerical integration on a 6 × 8 × 8 grid (μ = 7.41 cm^{-1}). The variation in the absorption correction for the three specimens was 3.9%, 6.0%, and 15.7%, respectively. A third-order polynominal, least-squares fitted to the variations of the standard reflections, was used to bring reflections to a common scale.

Table I. Crystallographic Information

	90 K	room temp
a, Å	5.7526 (5)	5.830 (3)
b, Å	10.3853 (9)	10.456 (4)
c, Å	11.868 (2)	12.028 (6)
β, deg	100.29 (1)	99.87 (2)
space group	$P2_1/n$	$P2_1/n$
Z	4	4
wavelength	0.710 69	0.710 69
temp, K	90	298
d_{calcd}, g cm^3	2.208	2.133

Symmetry-related reflections were averaged to yield respectively 3072, 5578, and 5681 independent reflections for the three separate data sets. Internal agreement indices on F^2 for the strongest reflections were 1.81%, 2.64%, and 1.46%, respectively. Full-matrix least-squares refinements, minimizing $\sum w(F_o - |F_c|)^2$, were performed for each data set including scale, positional, and thermal parameters and an isotropic type 1 Lorentzian extinction parameter as formulated by Becker and Coppens.[7] Positional parameters for the three sets agreed within the estimated standard deviations. The thermal parameters, however, indicated that the temperature of data set 3 was approximately 8° higher than that of data sets 1 and 2. In addition the three specimens exhibited differing amounts of extinction with mosaic spreads of 14.8, 52.8, and 27.2″ s of arc, respectively. The separate data sets were therefore combined in a single refinement in which positional and thermal parameters were refined from the full set of data, separate scale and isotropic extinction parameters were refined for each data set, and an overall temperature factor was refined for data set 3. The individual scale factors and isotropic extinction parameters and the overall thermal parameter were then applied to the corresponding unaveraged data sets (i.e., the data sets before being averaged over symmetry-equivalent reflections) to reduce the three sets of measurements to a common scale. After averaging of the combined data over symmetry-equivalent reflections, there remained 7283 independent reflections of which 5584 were greater than 3 times their estimated standard deviations. The internal agreement of the strongest reflections $[F^2 > 100\sigma(F^2)]$ was 2.62% on F^2.

Refinement. Full-angle refinement including an isotropic extinction parameter to describe remnant extinction effects showed no significant extinction to remain in the combined data set. Extinction was therefore not included in subsequent refinements. Positional and thermal parameters agreed within standard deviations with those determined from data sets 1 and 2 to which data set 3 was scaled. The weighted R factor on F for the full-angle refinement was 3.93%.

Parameters from an X-ray experiment may be biased by bonding effects present in low-order data. This bias can be reduced by use

(1) A. Hordvik, *Q. Rep. Sulfur Chem.*, **5**, 21 (1970).
(2) R. E. Rosenfeld, Jr., R. Parthasarathy, and J. D. Dunitz, *J. Am. Chem. Soc.*, **99**, 4860 (1977).
(3) T. N. Guru Row and R. Parthasarathy, private communication.
(4) T. N. Guru Row and P. Coppens, *Inorg. Chem.*, **17**, 1671 (1978).
(5) R. H. Blessing, P. Coppens, and P. Becker, *J. Appl. Crystallogr.*, **7**, 488 (1974).
(6) M. S. Lehmann and F. K. Larsen, *Acta Crystallogr., Sect. A*, **A30**, 580, (1974).
(7) (a) P. J. Becker and P. Coppens, *Acta Crystallogr., Sect. A*, **A30**, 129 (1974); (b) *ibid.*, **A30**, 148 (1974).

0020-1669/80/1319-2396$01.00/0

Table II. Details of Least-Squares Refinements[a]

	all data	HO	multipole
$((\sin\theta)/\lambda)_{min}$, Å^{-1}	0.0	0.70	0.0
no. of reflctns	5584	3710	5584
no. of parameters	100	100	246
weighted R^b on F, %	3.93	3.59	3.15
goodness of fit[c]	1.79	1.34	1.463
scale factor applied to F_o	0.3166 (3)	0.3180 (9)	0.3172 (3)

[a] Symmetries imposed on the deformation parameters: (a) m symmetry in the plane of the $S_4N_3^+$ ring; (b) m symmetry for N(4), O(2), and O(3); (c) mm symmetry for N(1); (d) no symmetry constraints on O(1); (e) S(1), S(2), S(3), and S(4) include deformations up to the hexadecapole level; (f) the remaining atoms include deformations up to the octapole level. [b] $R_w = 100[\Sigma w(F_o - |F_c|)^2/\Sigma wF_o^2]^{1/2}$. [c] $S = [\Sigma w(F_o - |F_c|)^2/(NO - NV)]^{1/2}$.

Table III. Bond Lengths (Å) and Angles (Deg)[a]

	room temp[b]	90 K (HO)[c]
S(1)-S(2)	2.082 (1)	2.0735 (4)
S(1)-N(2)	1.567 (3)	1.5663 (8)
S(2)-N(3)	1.565 (3)	1.5638 (8)
S(3)-N(1)	1.574 (3)	1.5709 (10)
S(3)-N(3)	1.543 (3)	1.5406 (8)
S(4)-N(1)	1.576 (3)	1.5743 (10)
S(4)-N(2)	1.546 (3)	1.5406 (9)
N(4)-O(1)	1.287 (3)	1.282 (1)[b]
N(4)-O(2)	1.273 (3)	1.258 (1)[b]
N(4)-O(3)	1.251 (4)	1.250 (1)[b]
S(1)···O(1)	2.620 (3)[c]	2.5844 (8)
S(2)···O(2)	2.695 (3)[c]	2.6525 (9)
S(1)-S(2)-N(3)	111.6 (1)	111.55 (3)
S(2)-N(3)-S(3)	152.2 (2)	152.21 (5)
N(3)-S(3)-N(1)	118.1 (2)	118.51 (4)
N(1)-S(4)-N(2)	119.7 (2)	119.13 (4)
S(3)-N(1)-S(4)	135.8 (2)	134.93 (6)
S(4)-N(2)-S(1)	150.8 (2)	151.06 (6)
N(2)-S(1)-S(2)	112.5 (2)	112.30 (3)
S(1)-O(1)-S(2)	45.82 (5)[c]	46.62 (1)
O(1)···S(1)-S(2)	69.01 (7)[c]	68.42 (2)
O(1)···S(2)-S(1)	65.17 (7)[c]	64.96 (2)
O(1)-N(4)-O(2)	119.7 (3)	119.05 (8)[b]
O(2)-N(4)-O(3)	122.0 (3)	121.43 (9)[b]
O(3)-N(4)-O(1)	118.3 (3)	119.50 (8)[b]
N(4)-O(1)···S(1)	109.9 (2)[c]	110.16 (5)
N(4)-O(1)···S(2)	111.8 (2)[c]	111.42 (5)

[a] Uncorrected NO bond lengths at room temperature are 1.264 (3), 1.220 (3), and 1.226 (3) Å and at low temperature are 1.273 (1), 1.238 (1), and 1.239 (1) Å. The difference between the thermally corrected bond lengths is thought to be due to uncertainties in the correction for the nitrate group. [b] Corrected for rigid-body motion. [c] Uncorrected for rigid-body motion.

of high-order (HO) refinements or alternatively by including nonspherical distortions of the spherical free atoms explicitly in the least-squares refinement. Both HO and multipole refinements of the combined data set were made. Details of these refinements are given in Table II. In all refinements a weighting scheme $w(F^2) = [\sigma^2(F^2) + (0.02F^2)^2]^{-1}$ was employed where $\sigma(F^2)$ was determined by using the method of McCandlish, Stout, and Andrews[8] and contains contributions from both counting statistics and scaling errors. Scattering factors for spherical atoms were as listed in ref 9. The anomalous dispersion factors of Cromer and Liberman[10] were applied for the sulfur atoms.

Results and Discussion

The packing arrangement within the unit cell is shown in Figure 1. Bond lengths and angles are listed in Table III and positional and thermal parameters from the least-squares refinements are given in Table IV.

Table IV

Low-Temperature Positional Parameters ($\times 10^5$)[a]

S(1)	17 819 (4)	44 247 (2)	12 199 (2)
	17 818 (3)	44 245 (2)	12 195 (2)
S(2)	51 589 (4)	39 012 (2)	20 113 (2)
	51 580 (3)	39 010 (2)	20 108 (2)
S(3)	49 309 (4)	11 078 (2)	13 127 (2)
	49 305 (3)	11 080 (2)	13 122 (2)
S(4)	2 275 (4)	18 565 (3)	1 767 (2)
	2 277 (3)	18 569 (2)	1 763 (2)
N(1)	24 148 (16)	9 452 (7)	5 545 (7)
	24 140 (12)	9 442 (6)	5 531 (6)
N(2)	3 686 (14)	32 659 (7)	5 884 (7)
	3 681 (11)	32 671 (6)	5 878 (6)
N(3)	56 316 (13)	24 370 (7)	18 430 (7)
	56 328 (10)	24 367 (6)	18 433 (6)
N(4)	48 878 (12)	70 577 (6)	14 868 (6)
	48 872 (10)	70 574 (6)	14 868 (5)
O(1)	40 980 (17)	63 652 (7)	22 194 (7)
	40 992 (22)	63 654 (10)	22 198 (9)
O(2)	57 673 (30)	65 254 (10)	7 295 (11)
	57 646 (17)	65 255 (10)	7 277 (8)
O(3)	47 969 (21)	82 468 (8)	15 569 (10)
	47 885 (14)	82 465 (8)	15 542 (9)

Thermal Parameters ($\times 10^4$)[b]

	U_{11}	U_{22}	U_{33}	U_{12}	U_{13}	U_{23}
S(1)	176 (1)	146 (1)	178 (1)	16 (1)	31 (1)	16 (1)
	174 (1)	144 (1)	177 (1)	17 (1)	32 (1)	15 (1)
S(2)	165 (1)	146 (1)	169 (1)	−18 (1)	8 (1)	−8 (1)
	164 (1)	145 (1)	169 (1)	−18 (1)	8 (1)	−9 (1)
S(3)	192 (1)	135 (1)	238 (1)	9 (1)	63 (1)	−2 (1)
	190 (1)	133 (1)	239 (1)	9 (1)	65 (1)	−2 (1)
S(4)	201 (1)	202 (1)	185 (1)	−56 (1)	−10 (1)	−3 (1)
	198 (1)	201 (1)	186 (1)	−57 (1)	−9 (1)	−4 (1)
N(1)	234 (3)	164 (2)	186 (2)	−34 (2)	52 (2)	−23 (2)
	229 (3)	163 (2)	190 (2)	−34 (2)	50 (2)	−25 (2)
N(2)	174 (2)	187 (2)	202 (2)	−9 (2)	2 (2)	22 (2)
	173 (2)	186 (2)	202 (2)	−9 (2)	2 (2)	22 (2)
N(3)	168 (2)	151 (2)	229 (2)	−1 (2)	16 (2)	−2 (2)
	167 (2)	148 (2)	231 (3)	−3 (2)	17 (2)	0 (2)
N(4)	185 (2)	150 (2)	143 (2)	−19 (2)	37 (2)	−1 (2)
	190 (2)	145 (2)	143 (2)	−20 (2)	42 (2)	−1 (2)
O(1)	311 (3)	184 (2)	185 (2)	−58 (2)	120 (2)	−15 (2)
	315 (4)	177 (4)	185 (3)	−52 (4)	119 (3)	−19 (3)
O(2)	546 (7)	231 (3)	277 (4)	−95 (3)	267 (4)	−73 (3)
	547 (6)	229 (4)	286 (3)	−101 (3)	272 (4)	−72 (3)
O(3)	337 (4)	144 (2)	310 (3)	40 (2)	92 (3)	29 (2)
	336 (4)	146 (3)	312 (3)	40 (2)	96 (3)	32 (2)

[a] Upper numbers refer to HO refinement; lower numbers to multipole refinement. Estimated standard deviations are in parentheses. [b] Upper numbers refer to HO refinement; lower numbers to multipole refinement. Estimated standard deviations are in brackets. The temperature factor is of the form $\exp[-2\pi^2(U_{11}h^2a^{*2} + \ldots + 2a^*b^*U_{12}hk + \ldots)]$.

The room-temperature bond lengths listed in Table III have been corrected for translational and librational components of rigid-body motion[11] as have the N–O bond lengths of the low-temperature structure. The remaining differences between the room-temperature and low-temperature NO bond lengths suggest that the rigid-body model is somewhat deficient in this case. An attempt to correct the low-temperature bond lengths in the $S_4N_3^+$ ring for rigid-body motion resulted in negative eigenvalues for the L tensor; hence only the uncorrected distances are given. Including the S tensor, which describes the correlation between the translational and librational components, gave negative eigenvalues for the L tensor in both the $S_4N_3^+$ and NO_3^- groups. We conclude that for the ring at least the rigid-body model is not valid at low temperatures. Within the $S_4N_3^+$ ring there is generally good agreement

(8) L. E. McCandlish, G. H. Stout, and L. C. Andrews, *Acta Crystallogr., Sect. A*, **A31**, 245 (1975).
(9) "International Tables for X-ray Crystallography", Vol. IV, Kynoch Press, Birmingham, England, 1974.
(10) D. T. Cromer and D. Liberman, *J. Chem. Phys.*, **53**, 1891 (1970).
(11) V. Schomaker and K. N. Trueblood, *Acta Crystallogr., Sect. B*, **B24**, 63 (1968).

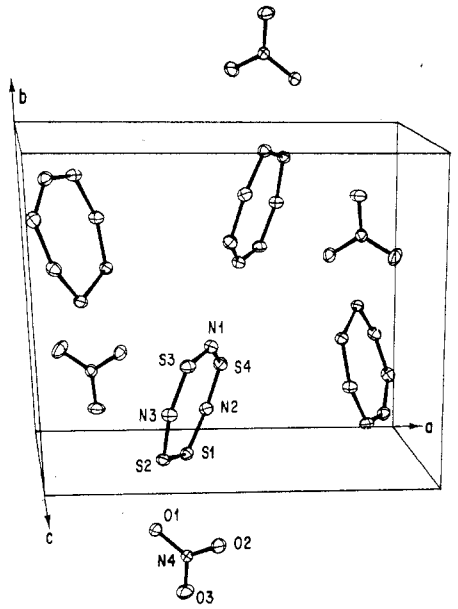

Figure 1. Packing arrangement in the unit cell showing 50% probability thermal ellipsoids and the atom-numbering scheme.

between the room-temperature corrected values and the low-temperature results, though the S_1–S_2 bond appears slightly shorter in the low-temperature structure. The decrease in the average S···O close contact separation on cooling from a room-temperature value of 2.657 Å to 2.618 Å is typical for intermolecular interactions and corresponds to what is expected from the contraction of the lattice parameters. This suggests the S···O contact to be a weak interaction.

The thiotrithiazyl ring is approximately planar with the weighted least-squares equation $2.95x + 2.50y - 10.71z - 0.34 = 0$. The maximum deviation from the plane is 0.038 (1) for N(2) while the O(1) atom of the nitrate group is 0.085 Å out of the plane of the ring. This in the plane approach of a nucleophile to a disulfide group has been observed in a large number of structures.[2,3,12] We note that the electronic interpretation of this interaction is confirmed by the orientation of the oxygen lone pair observed in this study. The weighted least-squares plane of the nitrate group is at an angle of 94.0° to that of the ring and lies approximately along the extension of the S(2)–O(1) vector.

Density Maps. Features of the electron density distribution are conveniently illustrated by use of maps which show the difference between the experimentally observed structure factors and those calculated from a superposition of spherical atoms. These maps are calculated by using parameters from the HO refinement. An extra cycle of refinement, varying only the scale factor and holding all other parameters at their HO values, is generally advocated to fix the scale for the calculation of density maps.[13] In the present case such a refinement changed the scale factor by less than 1σ; hence the HO scale factor was retained.

In the calculation of all density maps a $(\sin\theta)/\lambda$ cutoff of 0.80 $Å^{-1}$ was used to reduce the noise that may be introduced by a large number of weak high-order reflections. Care must be exercised in selecting an appropriate cutoff value as the resolution of sharp features in the density maps generally requires the inclusion of high-order data. The variation of bond and lone-pair peak densities in the thiotrithiazyl ring with $(\sin\theta)/\lambda$ cutoff is plotted in Figure 2 where it is seen that data

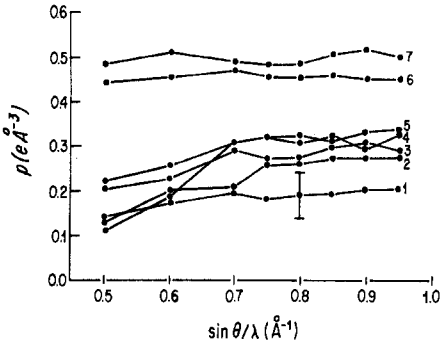

Figure 2. Variation of bond and lone-pair peak densities as a function of $(\sin\theta)/\lambda$ cutoff, within the thiotrithiazyl ring: 1, average of S_3 and S_4 lone pairs; 2, average S–N(1) peak densities; 3, average S_1, S_2 lone pairs; 4, S(1)–S(2) peak density; 5, N_1 lone pair; 6, average of S(2)–N(3) and S(1)–N(2) peak densities; 7, average of S(3)–N(3) and S(4)–N(2) peak densities.

beyond approximately 0.75 $Å^{-1}$ make no significant contributions to the peak heights in these regions. A similar variation was found for the bond and lone-pair peak densities in the nitrate ion.

Experimental X–X(HO) difference maps for the $S_4N_3^+$ ring and the NO_3^- ion are shown in Figures 3a and 4a. In order to assess the significance of features in the deformation maps it is important to consider the contributions from errors in the refined parameters.[14,15] Error maps (Figures 3b and 4b) were calculated as described by Rees[14] with use of an analytic method proposed by Stevens and Coppens.[16] The error calculated from the standard deviations of the observations alone gives rise to a uniform background of 0.05 e $Å^{-3}$. Contributions from errors in the refined parameters however peak at the atomic positions; hence features within approximately 0.35 Å of the sulfur sites and 0.25 Å of the nitrogen sites may be unreliably determined. The bonding in the S–N bonds is clearly covalent with large positive peaks between the atoms. These densities are elongated perpendicular to the bond axes and extend above and below the plane by approximately 0.5 Å. Sections bisecting the bond angle at the N atoms, and perpendicular to the ring (Figure 5), show that only the N(1) atom has a pronounced peak characteristic of lone-pair density.

The average value of the four S–N bonds involving N(2) and N(3) is 1.553 Å compared to a value of 1.573 Å for the S–N(1) bonds. These values agree favorably with the values of 1.558 and 1.584 Å predicted from a linear relationship between S–N distance and nitrogen bond angle derived by Banister.[17] This correlation may be interpreted as evidence for lone-pair donation into the adjacent S–N bonds, leading to a shift toward sp hybridization of N(2) and N(3).[17] Support for this argument is provided by the low lone-pair density of N(2) and N(3) relative to that on N(1). The N(1) lone-pair peak density of 0.32 e $Å^{-3}$ is in good agreement with the results of a low-temperature study of pyrazine.[18] The lone pair occurs at the expense of the N(1)–S bonds which have an average peak density of 0.27 e $Å^{-3}$ compared to an average value of 0.47 e $Å^{-3}$ for the other S–N bonds.

The presence of large negative areas around the sulfur atoms has not been observed in any of the other sulfur-containing compounds studied in this laboratory.[19–21] Sections perpen-

(12) O. Andreasen, A. C. Hazell, and R. G. Hazell, *Acta Crystallogr., Sect. B*, **B33**, 1109 (1977).
(13) E. D. Stevens and P. Coppens, *Acta Crystallogr., Sect. A*, **A31**, 612 (1975).
(14) B. Rees, *Acta Crystallogr., Sect. A*, **A32**, 483 (1976).
(15) E. D. Stevens, *Acta Crystallogr., Sect. B*, **B34**, 544 (1978).
(16) E. D. Stevens and P. Coppens, *Acta Crystallogr., Sect. A*, **A32**, 915 (1976).
(17) A. J. Banister, *Phosphorus Sulfur*, **5**, 147 (1978).
(18) G. DeWith, S. Harkema, and D. Feil, *Acta Crystallogr., Sect. A*, **A31**, 245 (1975).
(19) J. W. Bats, P. Coppens, and T. F. Koetzle, *Acta Crystallogr., Sect. B*, **B33**, 37 (1977).

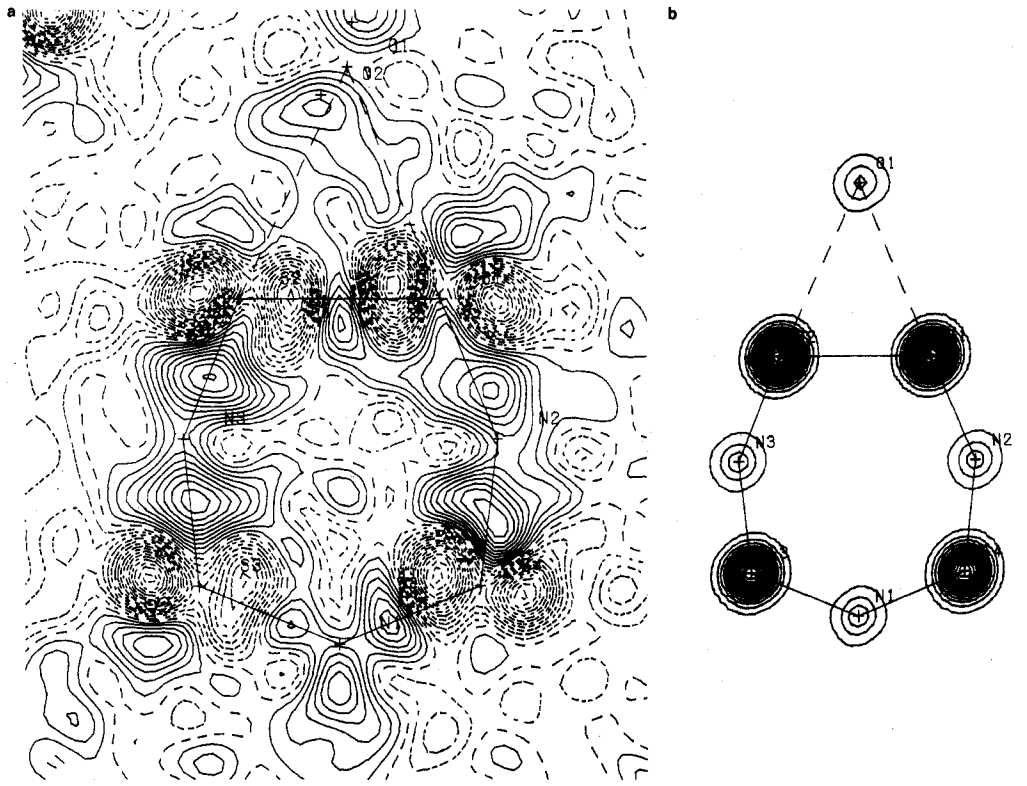

Figure 3. (a) Experimental deformation density in the plane of the thiotrithiazyl ring. Contours are at 0.05 e Å^{-3} with negative contours dashed. (b) Estimated error distribution of the deformation density in the molecular plane. Contours are at 0.025 e Å^{-3}. The general background is about 0.05 e Å^{-3}.

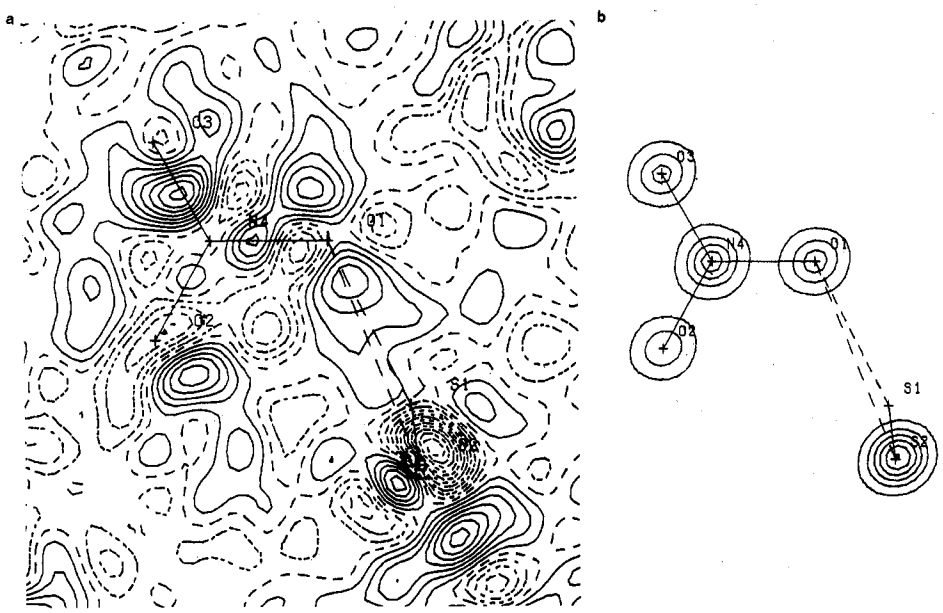

Figure 4. (a) Experimental deformation density and (b) estimated error distribution in the plane of the nitrate ion. Contours are as in Figure 3.

dicular to the plane of the ring and bisecting the bond angles show that the axis connecting the minima is tilted out of the plane (Figure 5). Bands of positive density extend above and below the plane of the ring in the sulfur lone-pair regions. Though there is little lone-pair density on S(4) in the molecular plane, density is observed above and below the plane near S(4). The lone pairs on the disulfide group are bent away from the SSN bond bisector toward the close-contact region. The S–S bond is bent with the centroid of the peak shifted toward the ring center. The peak density is 0.31 e Å^{-3} compared to a value of approximately 0.05 e Å^{-3} for the density at the center of the S–S bond in cyclic octasulfur (S–S bond length 2.050 Å) in which no maximum was observed at the bond midpoint. A section perpendicular to the ring and passing through the disulfide group (Figure 6) shows that the density extends above and below the plane, indicating some π character in the S–S bond. There is virtually no overlap density in the short interionic contact region between the O(1) atom and the disulfide

(20) P. Coppens, Y. W. Yang, R. H. Blessing, W. F. Cooper, and F. K. Larsen, *J. Am. Chem. Soc.*, **99**, 760 (1977).
(21) M. L. DeLucia and P. Coppens, *Inorg. Chem.*, **17**, 2336 (1978).

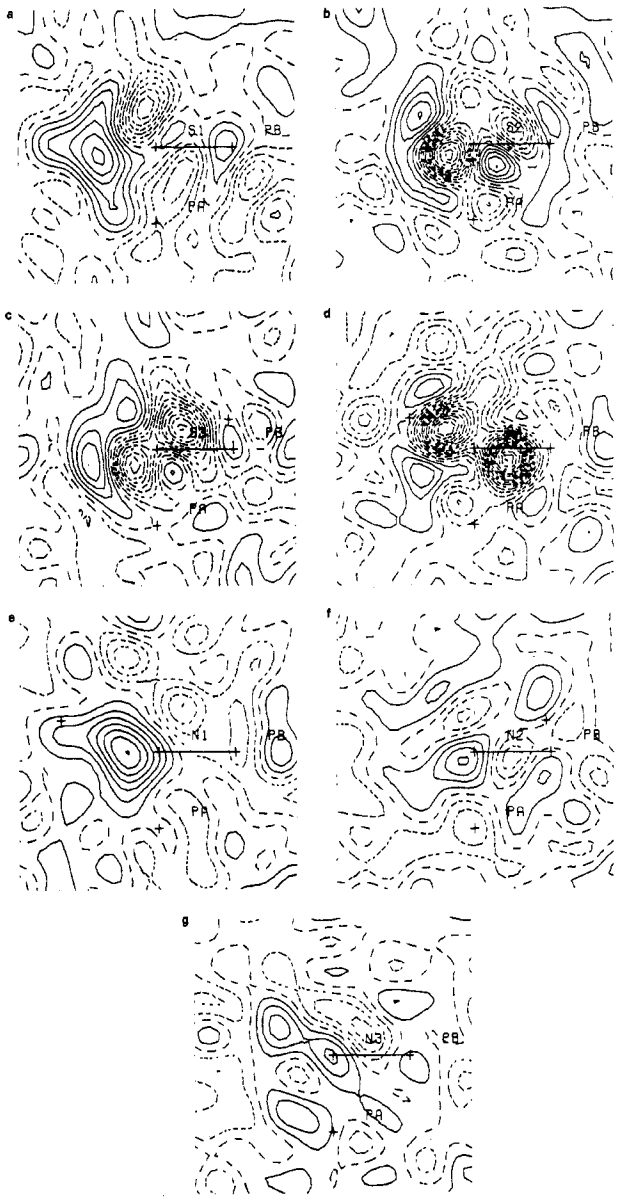

Figure 5. Sections through the atoms of the thiotrithiazyl ion, perpendicular to the plane of the ring and bisecting the bond angles. Contours are as in Figure 3a. The vector from the atom to point PB is the bond angle bisector in the plane of the ring and is directed to the ring interior. The vector from the atom to point PA is perpendicular to the plane of the ring and is in the same sense in all diagrams: (a) S(1), (b) S(2), (c) S(3), (d) S(4), (e) N(1), (f) N(2), (g) N(3).

group. However there is an apparent polarization of the oxygen lone-pair density toward the S(1) atom. This feature, though tentative, is consistent with the geometry of the S(1)···O(1)···S(2) arrangement for which the S(1)–O(1) separation is 0.07 Å shorter than the S(2)–O(1) distance. The effect of the close contact on the O(1) lone pair can be seen in Figure 4 where a rotation of the lone pairs into the plane of the $S_4N_3^+$ ring is clearly visible, in agreement with the nucleophilic nature of the nitrate group interactions.

Some uncertainty surrounds the nature of the N–O bonds. In both uronium nitrate[22] and *p*-nitropyridine *N*-oxide[23] no density was found in the N–O bonds. A recent study by Ohba,

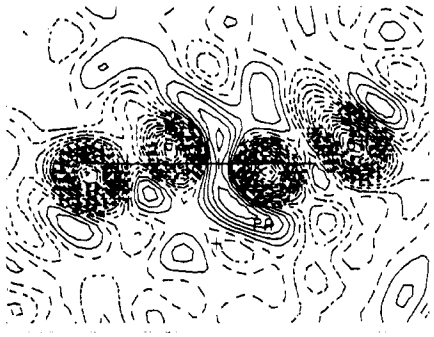

Figure 6. Section through the SS bond showing the extent of the disulfide bond density perpendicular to the plane of the thiotrithiazyl ring. Contours are as in Figure 3a.

Toriumi, Sato, and Saito[24] on the cobalt complex $K_2Na[Co(NO_2)_6]$, however, showed peak densities in the nitrite ligand of 0.32 e Å^{-3}, shifted slightly away from the bond axes. No obvious reason exists for the apparent difference between the N(4)–O(2) and N(4)–O(3) bond peak heights (0.08 and 0.42 e Å^{-3}, respectively) although we note that the N(4)–O(2) peak will be more strongly smeared by the larger thermal motion of O(2) in the direction perpendicular to the nitrate group plane. The lone pairs on the O(2) and O(3) atoms make an angle of approximately 90° with the NO bond. This result has been observed in several structures containing terminal oxygen atoms bonded to nitrogen. Coppens and Lehmann[23] have attributed the approximate sp hybridization of the oxygen atoms to an unfavorable balance between the energy required for s → p promotion and that regained by increased overlap in the σ bond.

Model Maps. Model deformation maps were calculated by using parameters determined from an all data multipole refinement. The static model maps provide details of the electron distribution at apparent infinite resolution, free of the effects of thermal motion. However, it is necessary to thermally smear the static deformation density and to calculate the resulting maps to the same resolution as the experimental ones if meaningful comparisons are to be made between model and experiment. The effect of thermally smearing the static density is shown in Figure 7. Residual densities, shown in Figure 8, highlight the remaining differences between the model and experimental maps and provide a guide to deficiencies in the deformation model used.

Within the $S_4N_3^+$ ring there is reasonable agreement. The density surrounding the N atoms appears to be well determined, and the S–N peak densities are within 1σ of the experimental values. The outstanding differences between the model and experimental maps are attributable to the density on the sulfur atoms. The deformation model does not appear flexible enough to simultaneously reproduce the large negative densities and the bond densities around the sulfur atoms. This may also account for the S–N bond densities being oriented more along the bond axes than found in the experimental map. While the negative peak densities are approximately a factor of 2 too small in the model map, their positions are in good agreement with the experimental ones. Apparently the negative peaks largely determine the radial dependence of the deformation functions on the sulfur atoms. This results in the features around the sulfurs being generally more contracted than in the experimental maps, particularly in the lone-pair regions.

Neither the S–S bond nor the close contact S···O region are reproduced well by the model. The peak density in the S–S bond has a value of 0.1 e Å^{-3} compared to an experimental

(22) S. Harkema, Thesis, Twente University of Technology, Enschede, The Netherlands, 1971.
(23) P. Coppens and M. S. Lehmann, *Acta Crystallogr., Sect. B*, **B32**, 1777 (1976).
(24) S. Ohba, K. Toriumi, S. Sato, and Y. Saito, *Acta Crystallogr., Sect. B*, **B34**, 3535 (1978).

Table V. Atomic and Molecular Charges (e) and Molecular Dipoles (D)

(i) Atomic Charges

	refinement			refinement	
	κ	multipole		κ	multipole
S(1)	−0.02 (9)	−0.13 (8)	N(3)	−0.26 (8)	−0.20 (8)
S(2)	−0.16 (9)	−0.17 (9)	N(4)	0.68 (8)	0.36 (13)
S(3)	0.21 (8)	0.32 (9)	O(1)	−0.04 (6)	−0.07 (7)
S(4)	0.21 (8)	0.36 (9)	O(2)	−0.15 (6)	−0.02 (7)
N(1)	−0.12 (6)	−0.30 (7)	O(3)	−0.03 (6)	0.05 (7)
N(2)	−0.32 (7)	−0.19 (7)			

(ii) Molecular Charges and Dipoles (− → +)[a]

		q	μ_x	μ_y	μ_z	$\lvert\mu\rvert$
$S_4N_3^+$	κ	−0.4 (1)	−4.4 (1.1)	−0.3 (3)	−0.1 (3)	3.6 (1.1)
	multipole	−0.3 (1)	−4.69 (1.2)	−0.05 (5)	−0.0 (2)	4.7 (1.3)
	direct integration[b]	0.2 (1)	−4.2 (4)	1.4 (3)	−1.0 (1)	4.5 (5)
NO_3^-	κ	0.4 (1)	0.2 (1)	−0.6 (3)	−0.0 (2)	0.6 (3)
	multipole	0.3 (1)	−0.9 (4)	−0.8 (4)	0.1 (2)	1.1 (6)
	direct integration[b]	−0.2 (1)	−1.1 (4)	−1.6 (5)	1.4 (1)	2.4 (6)

[a] Relative to center of mass. For $S_4N_3^+$ the x axis is the vector from N(1) through the midpoint of the S(1)–S(2) bond, and S(2), S(3), and N(3) have positive y coordinates. For NO_3^- the x axis is the vector from N(4) to O(1), and O(2) has a positive y coordinate. [b] Direct integration based on the following atomic radii to define a polyhedral volume:[29] S, 1.85 Å; N, 1.50 Å; O, 1.40 Å.

value of 0.31 e Å^{-3}. The localization of the deformation functions in general prevents the reproduction of the band of density extending from the close-contacted O(1) atom toward the S(1) atom.

In the nitrate group the model features are also slightly more contracted than in the map directly based on the experimental data (Figure 4). The orientation of the oxygen lone pairs is in agreement with the experimental result. The N(4)–O(1) peak density appears to be overestimated as are the lone-pair densities.

The sharpness of the model functions on S(1) and S(2) are the main reason behind the differences between the model and experimental maps for the $S_4N_3^+$ ring. In the case of the sulfur atoms this suggests that more flexible radial functions or density functions without the common separation of the angular and radial dependence are required to reproduce large features which peak at different distances from the atom. Further modifications of the deformation model may be required to achieve the delocalization of the atom-centered deformation functions necessary to reproduce the density in the S(1)···O(1)···S(2) close-contact region. In general, the present experience suggests that model maps should be treated with caution and not be accepted as the basis for further interpretation without careful comparison with experimental deformation maps and careful consideration of the residual maps.

Comparison with Theoretical Calculations. The theoretical static deformation density in planar S_4N_3Cl has been calculated by Johansen[25] from ab initio methods using a basis set which incorporated polarization functions. The calculated density in the disulfide group is in good quantitative agreement with the experimental result and shows the centroid of the positive peak displaced toward the ring center. The calculated peak density, however, is approximately 0.13 e Å^{-3}, in close agreement with an extended basis set calculation of the S_2^{2-} molecular ion by Stevens[26] (Figure 9), but much smaller than the experimental value. This difference may be due to an insufficient basis set in both calculations which results in energy convergence but not necessarily convergence of the calculated density or to limitations caused by data quality. The theoretical calculation also showed all nitrogen atoms to be very similar, with large densities in the lone-pair regions. This is in direct disagreement with the experimental map which shows N(1) as having lone-pair density but the chemically equivalent atoms N(2) and N(3) with little density in the lone-pair region. The calculated static lone-pair peak density on N(1) of approximately 1.0 e Å^{-3} agrees with the theoretical calculations by DeWith[27] on pyrazine. DeWith[27] has also calculated that the effect of thermal motion will decrease this

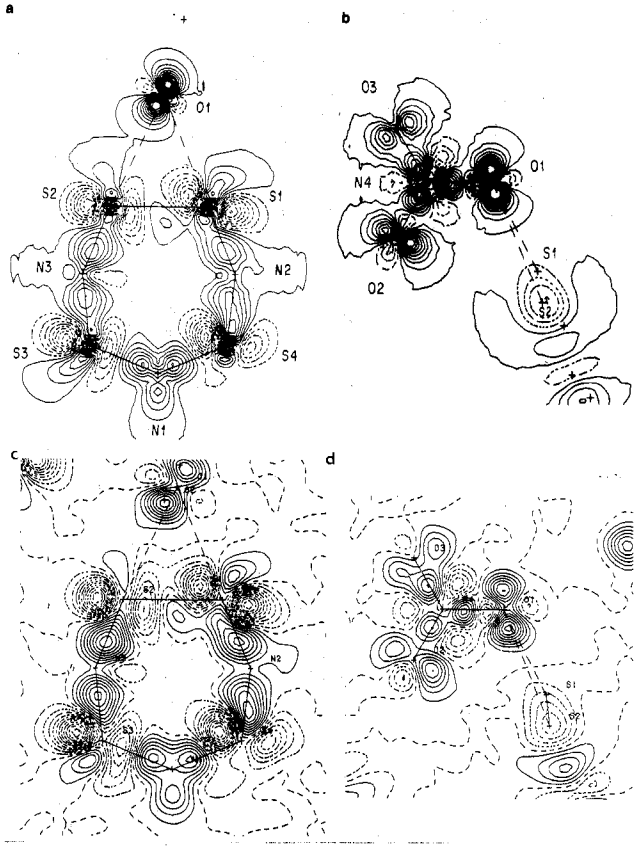

Figure 7. Effect of thermal smearing and series truncation on the least-squares fitted static multipole densities: a and b are static model densities for the thiotrithiazyl and nitrate ions; c and d are thermally smeared model densities calculated to the same resolution as the experimental deformation densities of Figures 3 and 4. Contours are as in Figure 3a.

(25) H. Johansen, private communication, 1979.
(26) E. D. Stevens, private communication, 1979.
(27) G. DeWith, Thesis, Twente University of Technology, Enschede, The Netherlands, 1977.

Figure 8. Residual densities in the planes after mulipole refinement for (a) thiotrithiazyl and (b) nitrate ion. Contours are as in Figure 3a.

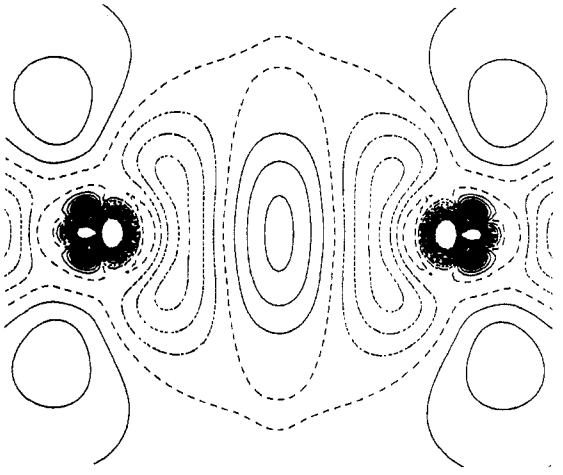

Figure 9. Theoretical static deformation density for the S_2^{2-} ion as calculated by Stevens[26] using an (11,8,2) Gaussian basis contracted to a (6,5,2) basis set. Atomic densities subtracted from the molecular density were calculated by using the same basis set. Contours are as in Figure 3a.

peak density to approximately 0.4 e Å^{-3}, in good agreement with the experimental value found here.

The experimental nitrate ion shows excess density in the NO bonds. This disagrees with the results of calculations by DeWith[27] using double-ζ and double-ζ plus d functions basis sets.

Net Charges and Dipole Moments. While the concept of atomic charges is not unambiguously defined in a molecule or solid, it is useful in giving an overall picture of the charge distribution. Atomic as well as molecular charges and molecular dipole moments (relative to the center of mass) have been derived from the results of the "κ" refinement, in which the atomic valence shells are allowed to expand or contract together with a variation of the valence shell population and the common structural parameters.[28] They have also been obtained from the multipole refinement discussed above and by direct integration of the experimental charge distribution using the polyhedral definition of the molecular volume.[29] Results of the various calculations are given in Table V.

The three methods all indicate a significant amount of charge transfer from the nitrate ion to the thiotrithiazyl ring, with the κ and multipole methods indicating a *negative* charge for the cation. The direct integration is in better agreement with conventional charge assignments, giving a small charge of 0.19 e. While the former result appears paradoxical, the small values of the ionic charges obtained with all three methods agree with the Pauling electroneutrality principle, confirmed also by other experimental studies, which states that atoms and ions in crystals are much closer to neutral than suggested by formal charges.

The dipole moments of $S_4N_3^+$ show that the ring is polarized with the disulfide group being negative. We note that this result is corroborated by the good qualitative agreement between the experimental density in the disulfide group and theoretical calculations on the negative S_2^{2-} ion by Stevens.[26] Negative net charges on sulfur atoms are not found in neutral sulfur–nitrogen species such as S_4N_4 in which the sulfur atoms were found to have net charges of about 0.3 e,[21] similar to values found for S(3) and S(4) in the present study. The negative charge on the disulfide group is in accord with the interpretation of the partial bonding in the close-contact region by the Hordvik[1] as being due to a partial transfer from the filled orbital on the O(1) atom to an empty orbital of the disulfide group.

Conclusions. The results of the present study give experimental evidence for the nature of the S···O interaction in agreement with the interpretation by Hordvik.[1] The interaction is weak, and the density in the close contact region is diffuse. Charge is transferred from the nitrate ion to the $S_4N_3^+$ ring and in particular to the disulfide group.

The residual density maps after the multipole refinement show that such multipole models must be used with caution and that a careful consideration of the residual density must be an integral part of any additional interpretation based on the multipole populations.

(28) P. Coppens, T. N. Guru Row, P. Leung, E. D. Stevens, P. J. Becker, and Y. W. Yang, *Acta Crystallogr., Sect. A*, **A35**, 63 (1979).

(29) P. Coppens and T. N. Guru Row, *Ann. N.Y. Acad Sci.*, **313**, 244 (1978).

The experimental and theoretical densities in the $S_4N_3^+$ ring are in good qualitative agreement except in the N(2) and N(3) lone-pair regions. Difference maps made perpendicular to the $S_4N_3^+$ ring and passing through N(2) and N(3) show some density in the lone-pair regions, but only N(1) exhibits a clear lone-pair peak. It is doubtful that the absence of lone-pair density on N(2) and N(3) is a function of the finite data size, particularly in view of the lone-pair density observed on N(1), though it could be related to the quality of the data set which is somewhat below the optimum that can be achieved. An alternative explanation for the disagreement may be that in such a large system containing second- and third-row atoms a very extended basis set is required to achieve convergence of the theoretical density.

Acknowledgment. The authors thank the donors of the Petroleum Research Fund, administered by the American Chemical Society, for support of this work. It is also a pleasure to acknowledge stimulating discussions with Dr. E. D. Stevens of this laboratory.

Registry No. $S_4N_3NO_3$, 12033-50-0.

Supplementary Material Available: A listing of observed and calculated structure factor amplitudes (24 pages). Ordering information is given on any current masthead page.

Contribution from the Laboratoire de Chimie de Coordination du CNRS, Associé à l'Université Paul Sabatier, F-31030 Toulouse, France

Reaction of Monodentate (Tertiary phosphine)nickel(II) Complexes $NiX_2(PR_3)_2$, $NiX_2(PMe_3)_3$, and $(NiX(PMe_3)_4)(BF_4)$ with Carbon Monoxide. Crystal and Molecular Structure of $NiI_2(CO)(PMe_3)_2$

CHRISTINE SAINT-JOLY, ALAIN MARI, ALAIN GLEIZES, MICHÈLE DARTIGUENAVE,* YVES DARTIGUENAVE, and JEAN GALY

Received April 24, 1979

Nickel(II) carbonyl complexes with the general formula $NiX_2(CO)(PR_3)_2$ and $[NiX(CO)(PMe_3)_3](BF_4)$ (X = halides; PR_3 = PMe_3, PEt_3, PMe_2Ph, $PMePh_2$, PPh_3) have been obtained either by addition of carbon monoxide on the tetracoordinate $NiX_2(PR_3)_2$ compounds or by substitution of a PMe_3 ligand in the pentacoordinate $NiX_2(PMe_3)_3$ and $[NiX(PMe_3)_4](BF_4)$ complexes, in normal conditions of temperature and pressure. The structure of $NiI_2(CO)(PMe_3)_2$ was determined from the three-dimensional X-ray data. Full-matrix least-squares refinement of the structure has led to a final conventional R factor on F of 0.027. The crystals have orthorhombic symmetry, space group *Pnma*, with four molecules per unit cell of dimensions a = 10.495 (1) Å, b = 10.744 (1) Å, and c = 14.047 (2) Å. The crystal structure consists of well-separated monomeric $NiI_2(CO)(PMe_3)_2$ molecules. The geometry around the Ni atom is trigonal bipyramidal. The two trimethylphosphine groups are in axial positions. The carbonyl ligand and the two iodine atoms are located in the equatorial plane. The Ni–C bond length of 1.728 (23) Å is the shortest reported Ni–CO distance. Solid-state and solution spectroscopic determinations (UV–visible, IR, $^{31}P(^1H)$ NMR) allow the characterization of all the carbonyl complexes as trigonal bipyramids of C_{2v} symmetry for $NiX_2(CO)(PR_3)_2$ and C_s for $[NiX(CO)(PMe_3)_3](BF_4)$, CO and X being located in the equatorial plane of the bipyramid. These complexes may be easily related to the probable intermediate in the formation of acylnickel(II) complexes, in carbonylation reactions. The solvent influence is discussed.

Introduction

Although numerous examples of insertion of carbon monoxide into transition-metal carbon bonds have been reported, such examples are rare in nickel(II) chemistry.[2] It is only recently that the first acylnickel(II) complexes have been synthesized: the square-planar tetracoordinate $NiX(COCH_3)(PMe_3)_2$ (X = Cl, Br, I)[3] and the pentacoordinate $[Ni(COR)np_3]^+$ (R = CH_3, C_2H_5, $CH_3C_6H_4$; np_3 = tris(2-(diphenylphosphino)ethyl)amine).[4] This is related to the easy reduction of Ni(II) complexes by CO, giving rise to Ni(0) species.

However, in a recent work on the carbonylation mechanism with d^8 nickel, palladium, and platinum phosphine complexes, it was reported that a probable mechanism for the carbonylation reaction was a pathway through a pentacoordinate d^8 intermediate, the first-step product being shown in reaction 1.[5] Such pentacoordinate carbonyl complexes have been isolated for M = Pt(II), and the authors suggested an identical mechanism for Ni(II) complexes.

$$MXR(PR_3)_2 + CO \rightleftharpoons MXR(CO)(PR_3)_2 \qquad (1)$$

The best way to test the validity of reaction 1 for Ni(II) complexes is to study the action of carbon monoxide with Ni(II) complexes in the absence of the alkyl ligand. Thus we have studied the action of carbon monoxide on the tetracoordinate $NiX_2(PR_3)_2$ and pentacoordinate $NiX_2(PMe_3)_3$ and $(NiX(PMe_3)_4)(BF_4)$ (X = halide; PR_3 = PMe_3, PEt_3, PMe_2Ph, $PMePh_2$, PPh_3). Prior to our work, only Ni(0) complexes have been obtained when CO was allowed to react with $NiX_2(PPh_3)_2$ and $NiX_2(PEt_3)_2$.[6,7] However, to our knowledge, three exceptions were reported: $NiI_2(CO)(PMe_3)_2$,[8] $NiI_2(CO)$(fdma) (fdma = 1,1′-bis(dimethylarsino)ferrocene,[9] and the cationic $(C_6Cl_5Ni(PR_3)_2(CO))(ClO_4)$.[10]

We report here the obtainment and characterization by the usual spectrochemical techniques, for all the nickel(II) complexes, of the corresponding pentacoordinate carbonyl com-

(1) (a) Based on the Ingenieur-Docteur Thesis of C.S.J., Université Paul Sabatier Toulouse, 1978. (b) *Adv. Chem. Ser.* **1979**, *No. 173*, 152.
(2) Jolly, P. W.; Wilke, G. "The Organic Chemistry of Nickel"; Academic Press: New York, 1974; Vol. 1.
(3) Klein, H. F.; Karsch, H. H. *Chem. Ber.* **1976**, *109*, 2524.
(4) Stoppioni, P.; Dapporto, P.; Sacconi, L. *Inorg. Chem.* **1978**, *17*, 718.
(5) Garrou, P. E.; Heck, R. F. *J. Am. Chem. Soc.* **1976**, *98*, 4115.
(6) Yamamoto, K. *Bull. Soc. Chem. Jpn.* **1954**, *27*, 516.
(7) Booth, G.; Chatt, J. *J. Chem. Soc. A* **1962**, 2099.
(8) Pankowski, M.; Bigorgne, M. *J. Organomet. Chem.* **1972**, *35*, 397.
(9) Bishop, J. J.; Davison, A. *Inorg. Chem.* **1971**, *10*, 832. Pierpont, G. G.; Eisenberg, R. *Ibid.* **1972**, *11*, 828.
(10) Wada, M.; Oguro, K. *Inorg. Chem.* **1976**, *15*, 2346.

0020-1669/80/1319-2403$01.00/0